Geophysical Research Letters

Surface Brightening in Eastern and Central China Since the Implementation of the Clean Air Action in 2013: Causes and Implications

Hongrong Shi[1,†] , Jinqiang Zhang[1,2,3,†] , Bin Zhao[4] , Xiangao Xia[1,2,3] , Bo Hu[5], Hongbin Chen[1,2,3], Jing Wei[6,7] , Mengqi Liu[1,3], Yuxuan Bian[8] , Disong Fu[1,3], Yu Gu[9] , and Kuo-Nan Liou[9]

[1]Key Laboratory of Middle Atmosphere and Global Environment Observation, Institute of Atmospheric Physics, Chinese Academy of Sciences, Beijing, China, [2]Collaborative Innovation Center on Forecast and Evaluation of Meteorological Disasters, Nanjing University of Information Science & Technology, Nanjing, China, [3]College of Earth and Planetary Science, University of Chinese Academy of Sciences, Beijing, China, [4]Pacific Northwest National Laboratory, Richland, WA, USA, [5]State Key Laboratory of Atmospheric Boundary Layer Physics and Atmospheric Chemistry, Institute of Atmospheric Physics, Chinese Academy of Sciences, Beijing, China, [6]State Key Laboratory of Remote Sensing Science, College of Global Change and Earth System Science, Beijing Normal University, Beijing, China, [7]Department of Atmospheric and Oceanic Science, Earth System Science 19 Interdisciplinary Center, University of Maryland, College Park, MD, USA, [8]State Key Laboratory of Severe Weather, Chinese Academy of Meteorological Sciences, Beijing, China, [9]Joint Institute for Regional Earth System Science and Engineering and Department of Atmospheric and Oceanic Sciences, University of California, Los Angeles, CA, USA

Abstract Surface brightening has been observed in China since 2005. However, it remains unclear whether the brightening has accelerated recently in response to the strictest ever air pollution control policies since 2013. By combining intensive surface and satellite observations, we find an unprecedented rapid increasing trend in surface solar radiation (SSR) of 0.70–1.16 W m^{-2} yr^{-1} over the eastern and central China for 2014–2019. Using a novel method to identify the relative contributions of aerosol and cloud radiative effects to the SSR trends, we find that the strongly declining aerosol radiative effect due to the strict air pollution controls is the main cause of the upward SSR trends; cloud variations should not be the main reason. Distinction exists in seasonal trends of SSR, with decreasing trends in winter and increasing trends in other seasons. Air pollution controls play an important role in regulating SSR, which has valuable implications for photovoltaic power generation.

Plain Language Summary Since 2013, China has implemented the strictest ever air pollution control policies, which resulted in substantial reductions in aerosol concentrations. However, it is still unclear how the recent stringent control measures affect the surface solar radiation (SSR), the primary energy source for the Earth system. Moreover, it remained a critical challenge in previous observational studies to properly disentangle the effect of aerosols on SSR changes from the effect of cloud variations. Using ground-based and satellite-based measurements, we find a dramatic increasing trend in SSR during 2014–2019 over the eastern and central China, which is among the world's fastest brightening in the last few decades. Further, we use a novel method to elucidate the relative contributions of the aerosol and cloud radiative effects to the SSR trends. The results show that the strongly declining aerosol radiative effect due to the strict control policies plays a dominant role in producing the upward SSR trends. Our finding indicates that the air pollution control actions can lead to not only considerable environmental and health improvements, but also increases in solar photovoltaic energy production. This is potentially an important cobenefit of air pollution controls in China which deserves more attention in future decision making.

1. Introduction

Surface solar radiation (SSR) is the Earth's primary natural source of energy. Variation in SSR can greatly influence the weather and climate (Wild et al., 2005), hydrological cycle (Ramanathan et al., 2001), carbon cycle (Bright et al., 2012), water evaporation (Roderick & Farquhar, 2002), and crop yield potential (Stanhill & Cohen, 2001). Furthermore, the SSR is essential for the solar photovoltaic (PV), which, as a potential

alternative to fossil fuels, has been expanding exponentially worldwide over the past two decades. PV capacity in China is expected to reach at least 400 GW by 2030, accounting for 10% of China's primary energy (CNREC, 2014; Sun et al., 2014). For better assessment and utility of the solar energy, it is important to well understand the interannual variations in SSR across China and the driving factors behind the variations.

The temporal trends in SSR have been investigated widely over China, particularly considering that China has serious and rapidly changing aerosol pollution which has a significant effect on SSR (Li et al., 2016; Liang & Xia, 2005; Xia et al., 2007). For example, by analyzing 40 years of surface radiation and sunshine duration measurements in China, Che et al. (2005) found that global and direct solar radiation decreased significantly while diffuse radiation increased over the latter half of the twentieth century. During this dimming period, Qian et al. (2006) found that the trends of total cloud cover and low cloud cover are both negative averaged over China, which is not likely to explain the decreasing SSR. By considering elevated aerosol optical depth, they speculated that increased air pollution may result in less solar radiation reaching the surface. By conducting transient sensitivity experiments based on a global climate model with sophisticated treatment of aerosol and cloud microphysics, Folini and Wild (2015) found that the dimming in eastern China between 1950 and 2000 was partly associated with increasing SO_2 and carbonaceous aerosol emissions. The above studies arrived at a consistent conclusion that SSR has decreased in the past century in China and an increase in aerosol loading is a plausible cause.

In contrast to the above earlier studies, a transition from dimming to brightening has been revealed around 2005. By analyzing the trend of SSR during 2005–2015, Li et al. (2018) found a brightening trend over East China, which was attributed to the aerosol optical depth (AOD) decrease and single scattering albedo (SSA) increase. Schwarz et al. (2020) implied that the surface brightening after 2005 in China was associated with the decreasing atmospheric absorption, but it was not clear which factors induced the decreasing absorption, such as aerosols, clouds, or other factors. Previous observation-based studies usually inferred the effect of aerosols on SSR trends by simply examining the relationships between the trends in SSR and aerosols. They seldom quantitatively evaluated the relative contributions of aerosols and clouds to the SSR trends, which prevented an accurate attribution of observed SSR trends to the two factors.

Since 2013, China has implemented the Air Pollution Prevention and Control Action Plan and a strengthened second-phase of the plan (also called "Defending the Blue Sky Action Plan") to set stricter targets than ever for the reduction of emissions of pollutants (Council, 2013, 2018). Consequently, annual mean $PM_{2.5}$ (particulate matter with diameter less than 2.5 μm) concentrations over major metropolitan regions dropped by 30–50% from 2013 to 2018, in response to substantial reductions in emissions of multiple pollutants, especially SO_2, primary $PM_{2.5}$, and NO_x (Ding et al., 2019; Zhai et al., 2019). Although the large decrease in $PM_{2.5}$ concentrations has been confirmed by observational and modeling studies (Leung et al., 2020; Wang et al., 2019), it is still unclear how the strict air pollution controls influence the SSR and how important they are relative to cloud variations. To address this question, we use SSR datasets from 2014 to 2019 over the eastern and central China (ECC) from extensive surface and satellite observations to explore the SSR temporal trends. Compared with previous observational studies, a major innovation of this study is that we elucidate the relative contributions of the aerosol and cloud radiative effects (AREs and CREs) to the SSR trends by exploiting the high-temporal-resolution surface observational data to identify scenes affected and unaffected by clouds and aerosols. The surface-based estimate of AREs and CREs are further intercompared with satellite-based estimates. The results are expected to help us better understand the impact of air pollution controls on radiation budget, regional climate, and solar photovoltaic energy production.

2. Region, Data, and Methods

2.1. ECC Region

We focus on the ECC region (21–41°N, 102–122°E), where the aerosol loadings are extremely high and therefore strict control measures have been taken since 2013. The ECC domain covers most of China's major metropolitan regions, including the North China Plain, the Yangtze River Delta, and the Pearl River Delta. The research domain and observation stations are shown in Figure S1.
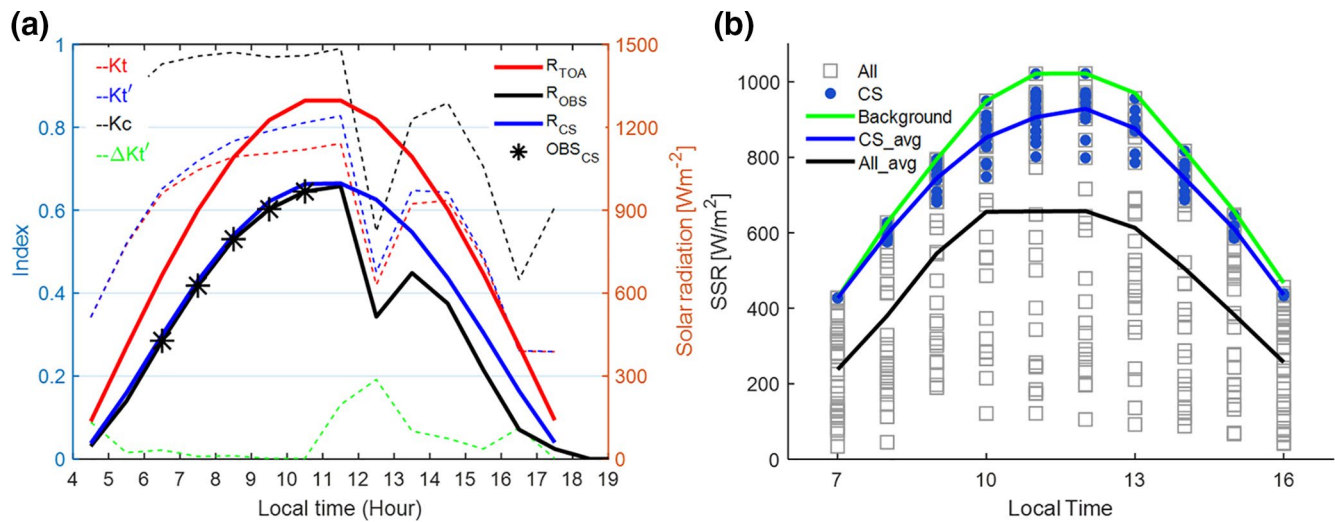
Figure 1. Illustration of (a) the clear-sky identification method and (b) the determination of monthly aerosol radiative effect (ARE) and cloud radiative effect (CRE) based on hourly observations from CERN network. The data of this case are from the CSA station (31.53°N, 120.68°E, see location in Figure S1) on June 15, 2018 (a) and during the period of June 2018 (b). In left panel, solid lines are downward solar radiation at top of atmosphere (R_{TOA} in red), SSR (R_{OBS} in black), and clear-sky SSR (R_{CS} in blue). Dashed lines are the indices used to identify the clear-sky SSR. Black stars represent identified clear-sky conditions. K_t is the ratio of R_{OBS} to R_{TOA}. K_t' is the modified K_t proposed by Perez et al. (1990). K_c is the ratio of R_{OBS} to R_{CS}. $\Delta K_t'$ is the variation of the K_t'. The scenes marked by stars are identified as the clear-sky conditions ($K_t < 0.82$; $0.65 < K_t' < 1$; $K_c > 0.65$; $\Delta K_t' < 0.05$). In right panel, gray squares are hourly SSR values over 1 month. Blue dots are clear-sky SSR. ARE is determined by the difference between the background clear-sky value (clear-sky without aerosols, green line) and mean clear-sky value (clear-sky with aerosols, blue line). CRE is calculated as the difference between averaged all-sky (black line) and clear-sky (blue line) SSR measurements. CERN, Chinese Ecosystem Research Network; SSR, surface solar radiation.

2.2. Surface Observational Data and Clear-Sky Screening Method

SSR data during 2014–2019 at 17 stations of the Chinese Ecosystem Research Network (CERN) over ECC is used. The CERN network was established to investigate the surface radiation budget and its spatial and temporal variations in China (Liu et al., 2017; Shi et al., 2018). The CM11 pyranometers with an accuracy of 3% are used for SSR measurement (Hu et al., 2007). The pyranometers are calibrated each year using the "alternate method" (Forgan, 1996). Quality control of SSR is performed based on two main principles: (i) SSR is smaller than the extraterrestrial global solar radiation, and (ii) SSR is larger than the expected minimum values ($10\ W\ m^{-2}$) in overcast conditions (Liu et al., 2017). The data failed the quality control would be treated as missing value. Quality controlled hourly SSR is integrated to calculate daily mean SSR, in which the number of missing hourly daytime values must be less than 3. Subsequently, monthly SSR is calculated based on daily SSR if the percentage of valid daily values exceeds 30%.

To investigate whether the SSR varying trends are associated with aerosols or clouds, the aerosol radiation effect (ARE) and cloud radiation effect (CRE) on the SSRs are analyzed under clear-sky and all-sky conditions, respectively. By calculating and examining several clear-sky indices, clear-sky screening procedure is applied to hourly CERN SSRs to detect clear-sky scenes. An hourly SSR value is regarded as clear-sky if it meets the following four criteria simultaneously; otherwise it is treated as cloudy condition. First, K_t, the ratio of SSR to extraterrestrial solar radiation at the top of the atmosphere (TOA), should not exceed 0.82. Second, the K_t', modified K_t proposed by Perez et al. (1990), should be between 0.65 and 1.0. Third, the variability of K_t' within 3 h should not exceed 0.05. Fourth, K_c, the ratio of SSR to the expected clear-sky SSR, should exceed 0.65. Here, the expected clear-sky SSR is calculated from a parameterized radiative transfer model named REST-2 (Gueymard, 2008), which was derived by a minimal water vapor pressure (0.25 hPa) and a background-level aerosol optical depth (AOD) of 0.1 at 550 nm. As an example, Figure 1a illustrates how clear-sky scenes at the CSA station (31.53°N, 120.68°E, see location in Figure S1) on June 15, 2018 are identified by using the above tests. Results show that the method can effectively screen out scenes with SSR reduction caused by clouds (e.g., the abrupt SSR reduction between 12:00 and 13:00 local time due to the clouds blocking the sunlight in Figure 1a) and hence identify clear-sky conditions.

Similar to the method in (Li et al., 2007), clear-sky SSR measurements are analyzed on a monthly basis to determine the monthly mean AREs. To account for the aerosol effects on SSR, all clear-sky data in each month are used to determine the background clear-sky values (clear-sky without aerosols) and mean clear-sky value (clear-sky with aerosols) and then to estimate monthly AREs. Specifically, the highest hourly values within a month (the outer envelope of hourly cloud-free SSR values) are considered to be the clear-sky background (green line in Figure 1b). The monthly mean hourly clear-sky values are considered to be the clear-sky values with the aerosol effects (blue line in Figure 1b). AREs here are calculated as the differences between the two averaged over 24 h. Similarly, CRE is calculated as the daily mean difference between all-sky (black line in Figure 1b) and clear-sky (blue line in Figure 1b) SSR measurements. Then the daily AREs and CREs are aggregated to monthly, seasonal, and annual AREs. We also do a sensitivity scenario with changed clear-sky screen criteria. The results indicate that, while the uncertainty may affect the magnitude of ARE and CRE (Li & Trishchenko, 2001), it has a smaller influence on their interannual trends (details in Text S1 and Figure S2).

2.3. Satellite Data

The Clouds and the Earth's Radiant Energy System (CERES) instrument, deployed on the Earth Observing System's Terra and Aqua satellite platforms, consists of a scanning radiometer collecting radiometric measurements in the shortwave (0.3–5 μm), longwave (8–12 μm), and broadband (0.3–100 μm) channels (Wielicki, 1996). The National Aeronautics and Space Administration CERES_SYN1deg_Ed4.1 hourly averaged SSR products during 2014–2019 are used (Doelling et al., 2016). Surface fluxes in SYN1deg are derived from TOA fluxes combined with aerosol and cloud properties derived from Moderate Resolution Imaging Spectroradiometer (MODIS) and geostationary satellites (GEO), where each geostationary satellite instrument is calibrated against MODIS (Doelling et al., 2013). CERES_SYN1deg_Ed4.1 provides SSR data at four types of atmospheric conditions: (i) all-sky, (ii) clear-sky, (iii) all-sky without aerosols, and (iv) clear-sky without aerosols (pristine). Type (iii) conditions are computed by removing aerosols from the all-sky computations. Type (iv) conditions are computed by removing aerosols from clear-sky computations, that is, including only molecular scattering and absorption. In this study, we calculate the impact of aerosols on SSR (i.e. ARE) using the difference between clear-sky without aerosols and clear-sky (with aerosols) conditions. Similarly, we calculate the impact of clouds (i.e. CRE) using the difference between all-sky and clear-sky conditions.

Previous studies concluded that CERES_SYN1deg, with substantially less average biases, outperforms other satellite-derived datasets, such as the International Satellite Cloud Climatology Project Radiative Flux Data (ISCCP), the Global Energy and Water Exchanges Surface Radiation Budget dataset 3.0 (GEWEX), and the Modern-Era Retrospective Analysis for Research and Applications (MERRA) (Li et al., 2017; Rutan et al., 2015). Here, we validate daily SSR data against CERN pyranometer measurements during 2014–2019, which showed that the mean bias (MB: CERES minus CERN), mean absolute bias (MAB), root mean square error (RMSE), and correlation coefficient are -10.35 W m^{-2}, 26.16 W m^{-2}, 32.43 W m^{-2}, and 0.94 W m^{-2}, respectively (shown in Figure S3). These results indicate a reasonable performance of CERES SSR, which is generally consistent with previous studies (Feng & Wang, 2018; Wang et al., 2015). Two datasets (CERN and CERES) inevitably have slight differences because of their different observation approaches and retrieval methods, which cause certain differences in the magnitude of trends derived from these two datasets. Nevertheless, a significant increasing pattern of SSR is consistently presented by these two-independent data sources, which strengthens the reliability of our results.

We utilize AOD (550 nm) and cloud fraction (CF) observations from the MODIS onboard Terra and Aqua satellites, each of which provides near-daily global coverage. Both AOD and CF are obtained from the Level 3 Atmosphere products (MOD08, Collection 6.1 for Terra and MYD08, Collection 6.1 for Aqua). Comparison of MODIS-retrieved AOD and CF with other ground and satellite-based datasets showed reasonable agreement (Harris et al., 2014).

We employ a high-resolution (1 km) and high-quality PM$_{2.5}$ dataset for China generated from MODIS AOD dataset using the Space-Time Extra-Trees (STET) model (Wei et al., 2020, 2021). The PM$_{2.5}$ estimates agree well with ground measurements (cross-validation R^2: 0.86–0.90; RMSE: 10.0–18.4 μg/m^3 from 2013 to 2018) (Wei et al., 2021). We calculate the PM$_{2.5}$ trends from the monthly PM$_{2.5}$ anomalies during 2014–2019 across China (Wei et al., 2019).
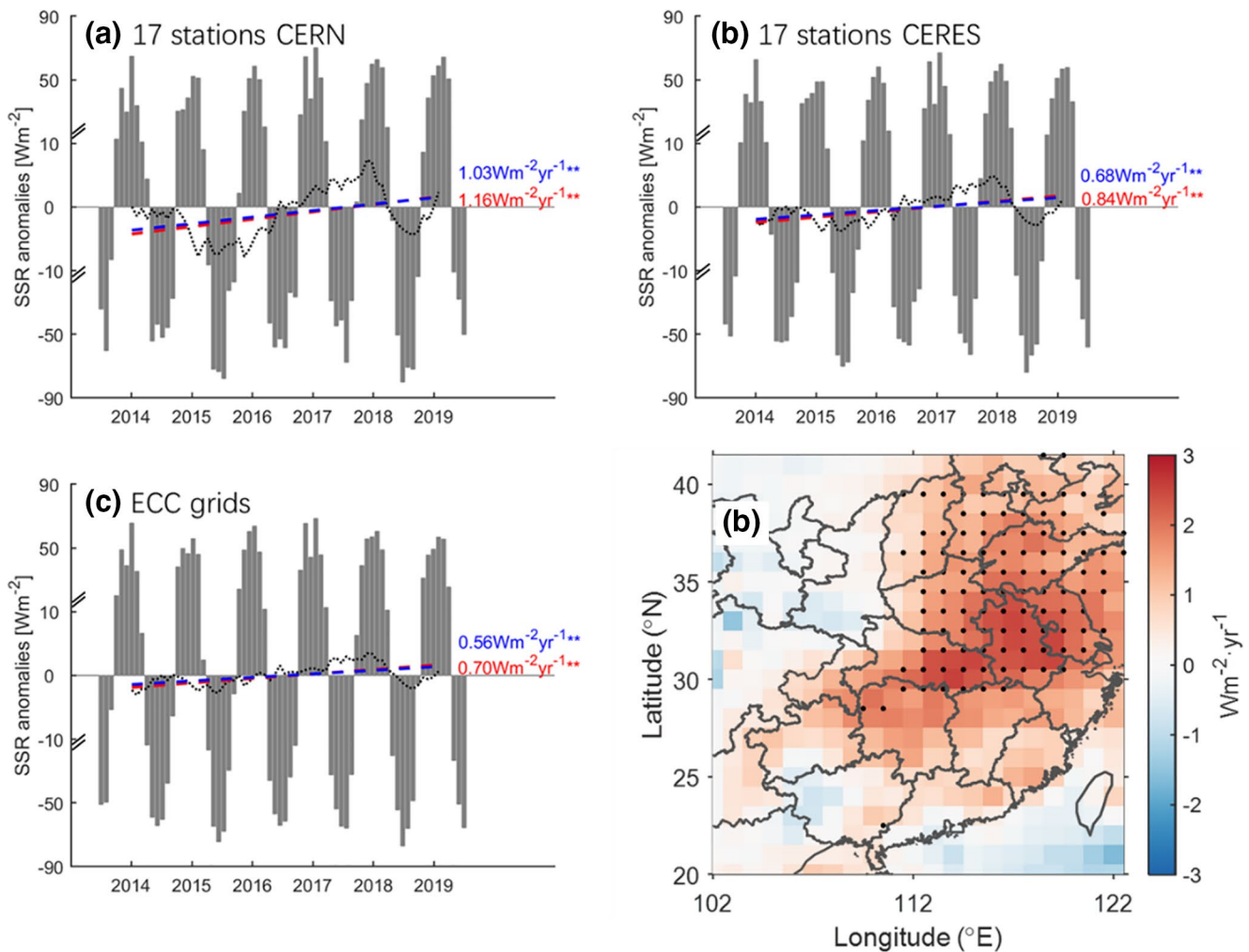
Figure 2. Trends of anomaly SSRs during 2014–2019 over the eastern and Central China (ECC). (a) Monthly SSR averaged across 17 stations from CERN surface observations in ECC. (b) Monthly SSR averaged across 17 stations from CERES satellite retrievals in ECC. (c) Monthly SSR averaged over the entire ECC from CERES. (d) Spatial distribution of the trends of SSR in ECC. Black dotted lines are moving averaged value with 12-months window. Dash lines in blue represent the regression lines and those in red represent the Sen's slopes (** marked as the significance level $p < 0.05$). Black dots in (d) indicate that the trend is above 95% significance level with M-k test. The inhomogeneous y-axes plotting scales is used to an individual panel in (a)–(c). CERES, Clouds and the Earth's Radiant Energy System; SSR, surface solar radiation; CERN, Chinese Ecosystem Research Network.

2.4. Statistical Method

The interannual trends with statistical significance at the 0.05 level are determined using two methods: the simple linear regression associated with Student's t-test and the Sen's slope associated with Mann-Kendall (M-k) test. The simple linear regression is a popular method to quantify trends of time series. The Sen's slope associated with M-k test is a nonparametric method for identifying a monotonic trend of a time series with any skewed distribution (Mann, 1945). We thus perform both parametric and nonparametric tests to ensure that the two methods produce consistent results.

3. Results and Discussion

3.1. Observed Trend in SSR

Figures 2a and 2b show the trends of SSR anomalies at 17 stations over ECC during 2014–2019. For both surface and satellite datasets, a statistically significant increasing tendency is revealed by the SSRs with Sen's slopes of 1.16 W m^{-2} yr^{-1} for CERN observation and 0.84 W m^{-2} yr^{-1} for CERES measurement,

respectively. Although two datasets have slight difference in trends, a significant increasing pattern of SSR is consistent by two-independent data sources. The corresponding regression slopes are 1.03 W m^{-2} yr^{-1} for CERN and 0.68 W m^{-2} yr^{-1} for CERES, respectively. We further examine the satellite-derived SSRs averaged over the entire ECC domain (Figure 2c), which also present a significant positive trend with a Sen's slope of 0.70 W m^{-2} yr^{-1} and a regression slope of 0.56 W m^{-2} yr^{-1}, similar to the trends at the 17 observational stations over ECC.

Figure 2d shows the spatial distribution of the trends of annual mean SSR from the CERES dataset. The SSR shows an increase over most of ECC, with the most significant increase occurring in northern and central parts of the domain (≥2 W m^{-2} yr^{-1}). However, the SSRs over southern and western parts of ECC show insignificant increases or even a weak decline in certain grids.

As mentioned earlier, a "dimming" trend (i.e., decrease in SSR) has been reported in China until 2005 when the "dimming" shifted to "brightening" over East China (Li et al., 2018; Schwarz et al., 2020). To put our results into the context of a longer timescale, we display the time series of annual mean SSR from CERN and CERES datasets averaged across 17 stations in ECC during 2005–2019 in Figure S4. Overall, the SSRs during 2005–2019 showed a weaker increase with regression slopes of 0.27 W m^{-2} yr^{-1} for CERN observations and 0.11 W m^{-2} yr^{-1} for CERES measurements. In contrast, a much larger increase was revealed after 2013, as described above. The difference in SSR trends between these two periods indicates that the recovery of SSR in China has accelerated, which probably benefits from the stricter air pollution control action after 2013. It has been well-documented that the SSRs in Europe and United States have been increasing gradually in the last 2-3 decades with a trend of round 0.3 W m^{-2} yr^{-1} in Europe for 1985–2012 (Sanchez-Lorenzo et al., 2015) and 0.6 W m^{-2} yr^{-1} in United States for 1996–2011 (Augustine & Dutton, 2013). Therefore, during 2014–2019, ECC has witnessed some of the world's highly rapid brightening in the last few decades.

The trends of seasonal mean SSR anomalies are presented in Table S1. Both the surface observations and satellite measurements show increasing trends with statistical significance in summer but decreasing trends in winter. The seasonal mean SSRs from CERN stations have Sen's slopes of −3.66 W m^{-2} yr^{-1} in winter, 1.87 W m^{-2} yr^{-1} in spring, 3.00 W m^{-2} yr^{-1} in summer, and 3.99 W m^{-2} yr^{-1} in autumn. Similarly, the co-located CERES observations have Sen's slopes of −1.22, 2.66, 2.05, and 2.36 W m^{-2} yr^{-1} in the four seasons. The regression slopes are very similar to the corresponding Sen's slopes, though the magnitude can be slightly different. In summary, our results show positive annual SSRs trends during 2014–2019, and the trends are positive in all seasons except winter.

3.2. Drivers for the SSR Varying Trend

The two major factors affecting SSR—aerosols and clouds are examined in this section to better understand the SSR varying trends. Figure 3 shows the trends of annual mean ARE, CRE, AOD, and CF anomalies from ground-based and satellite-based datasets during 2014–2019 over the ECC domain. Details of magnitudes of ARE and CRE are in Text S2 and Figure S5. The annual mean AREs averaged across 17 stations exhibit declining trends with regression slopes of −0.24 W m^{-2} yr^{-1} for CERN and −0.70 W m^{-2} yr^{-1} for CERES (Figures 3a and 3b). Similarly, the satellite-derived ARE averaged over the entire ECC domain (Figure 3c) shows a significant negative trend with a regression slope of −0.55 W m^{-2} yr^{-1}. The Sen's slopes of AREs are close to the regression slopes, confirming the aforementioned trends. The change in ARE is closely related to the change in aerosol loadings. During 2014–2019, AOD averaged over the ECC domain has a significant declining trend with a regression slope of −0.03 yr^{-1} (Figure 3d). Meanwhile, surface PM$_{2.5}$ concentrations have also decreased substantially during this period (Leung et al., 2020; Zhai et al., 2019). It has been well recognized that the large decrease in PM$_{2.5}$ and AOD during this period is mainly caused by substantial emission reductions associated with stringent control policies (Ding et al., 2019; Leung et al., 2020; Zhang et al., 2019). Therefore, the decreasing trends in ARE largely benefit from the decrease in aerosol loadings due to recent substantial emissions reductions in China.

The annual CREs (in Figures 3e–3g) from both surface and satellite measurements show insignificant trends. For surface measurements, the annual mean CRE averaged across 17 stations has negligibly small slopes (regression slope of −0.02 W m^{-2} yr^{-1} and Sen's slope of 0.09 W m^{-2} yr^{-1}). As a result, the significantly
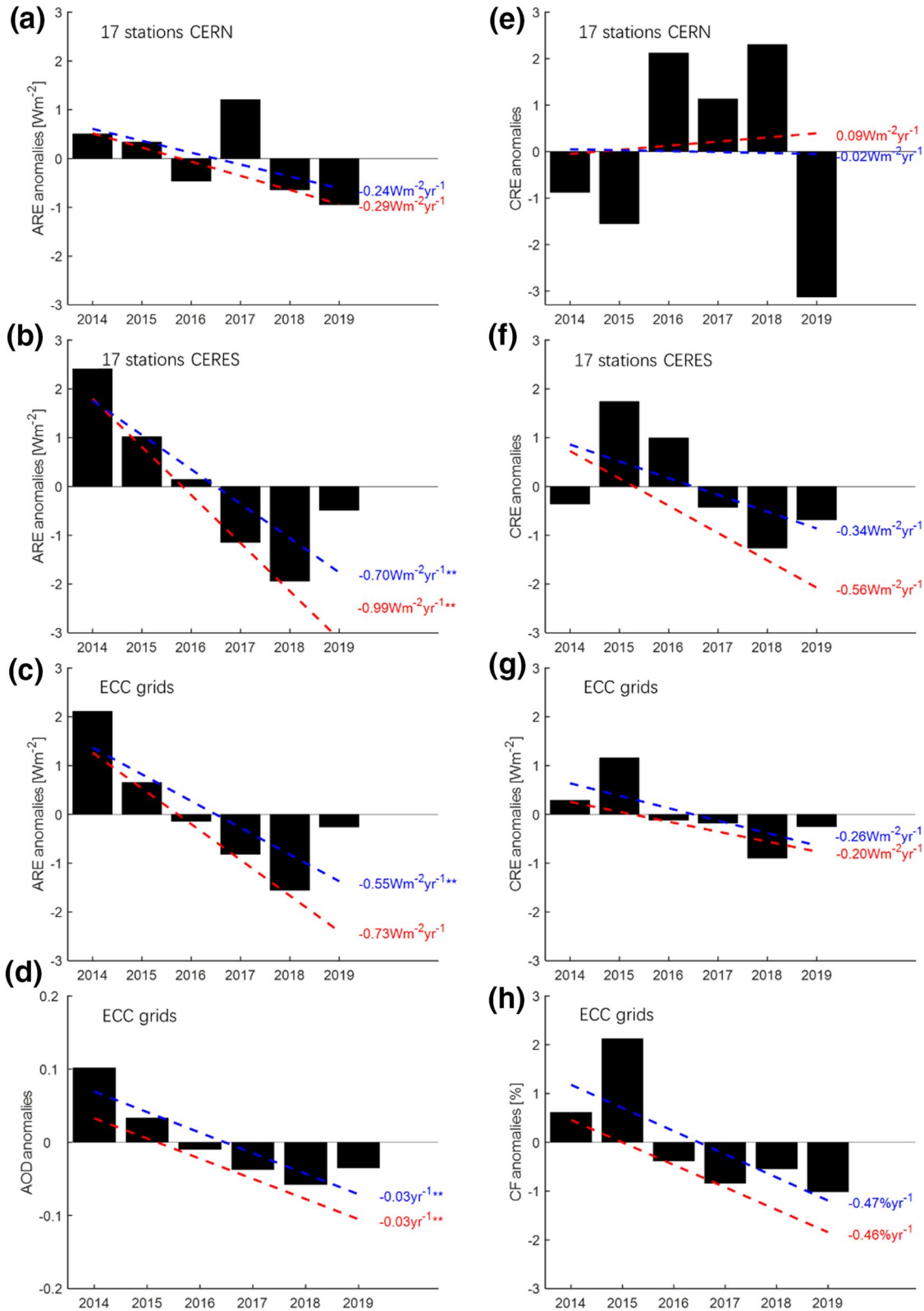
Figure 3. Annual trends of anomaly aerosol radiative effect (ARE), cloud radiative effect (CRE), aerosol optical depth (AOD), and cloud fraction (CF) from CERN surface observations and CERES and MODIS satellite measurements during 2014–2019 over the ECC. (a), (e) ARE and CRE trends from CERN observations averaged over 17 stations across ECC. (b), (f) ARE and CRE from CERES averaged over 17 stations across ECC. (c), (g) ARE and CRE from CERES averaged over the entire ECC. (d), (h) The AOD and CF from MODIS averaged over the entire ECC. Dash lines in blue represent the regression lines and those in red represent the Sen's slopes (** marked as the significance level $p < 0.05$). CERN, Chinese Ecosystem Research Network; CERES, Clouds and the Earth's Radiant Energy System; MODIS, Moderate Resolution Imaging Spectroradiometer; ECC, eastern and central China.
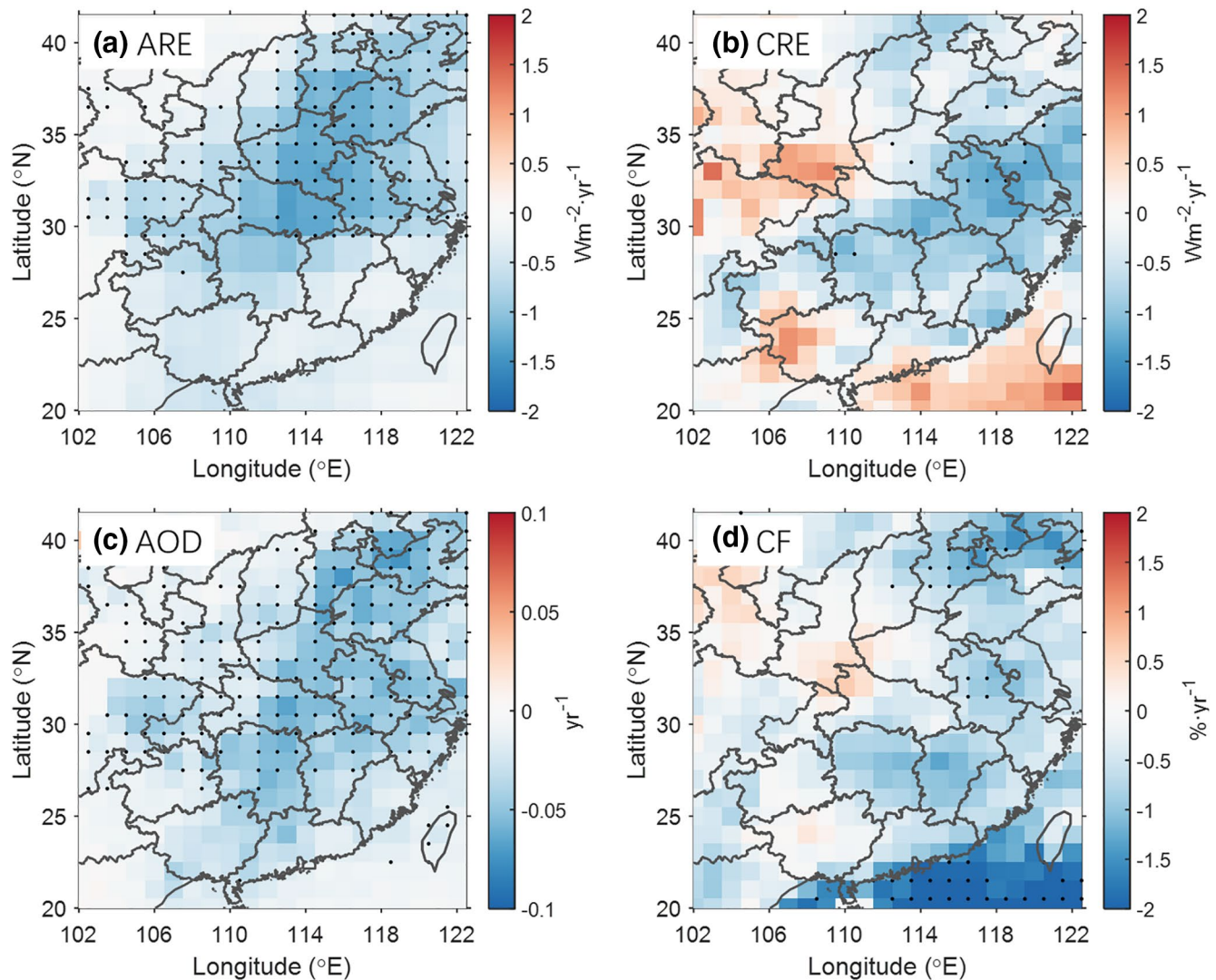
Figure 4. Spatial distribution of trends in (a) aerosol radiative effect (ARE), (b) cloud radiation effect (CRE) derived from CERES measurements, and (c) aerosol optical depth (AOD) and (d) cloud fraction (CF) from MOIDS measurements during 2014–2019. Black dots indicate that the trend is above 95% significance level with M-k test. CERES, Clouds and the Earth's Radiant Energy System; MODIS, Moderate Resolution Imaging Spectroradiometer.

decreasing ARE acts as the dominant driver for the increasing trends in SSR. For the satellite measurements, the CREs averaged across 17 stations or over the entire ECC domain both have negative slopes (regression slopes of -0.34 W m^{-2} yr^{-1} for 17 stations and -0.26 W m^{-2} yr^{-1} for the ECC domain), but the slopes are not statistically significant because of large interannual fluctuations. This is consistent with the insignificant decreasing trend in satellite-observed annual mean CF (Figure 3h). Since the CRE trends are insignificant and have smaller magnitude than the ARE trends, the satellite-based results also indicate that the strongly declining ARE plays a dominant role in producing the upward annual SSR trends.

Figure 4 shows the spatial distribution of the trends of annual ARE, CRE, AOD, and CF from 2014 to 2019 in the ECC domain. The ARE decreases almost everywhere across the ECC domain, with statistically significant decreases of approximately -2 W m^{-2} yr^{-1} over northern and central parts of the domain where the prominent AOD decreases occur. Similarly, large rate of aerosol loading change happened in the same domain parts due to the strict air pollution controls (Figure S6). The CRE decreases to some extent in a majority of the domain and increases in some other parts; however, the trends are generally insignificant except for a few scattered points. The highly inhomogeneous distribution of CRE leads to an overall effect that is much smaller than ARE, though the magnitude of CRE can be comparable to ARE at certain

locations. Again, these results confirm our conclusion that clouds should not be the main reason for the upward trends of SSRs in ECC.

In the previous section, we have shown different trends of seasonal mean SSRs, with decreasing trends in winter and increasing trends in other seasons. This can be explained by the following seasonal differences in CRE and ARE. The CRE decreases in spring, summer, and autumn but increases in winter (with regression slope of 1.26 W m^{-2} yr^{-1} for 17 stations from CERN and 1.64 W m^{-2} yr^{-1} for CERES), largely because of opposite CF trends in winter and other seasons during the period studied (Table S1). The ARE exhibits decreasing trends in all seasons, but the trends are much weaker in winter (with a regression slope of -0.16 W m^{-2} yr^{-1} for CERN and -0.33 W m^{-2} yr^{-1} for CERES) than in summer (-0.53 W m^{-2} yr^{-1} for CERN and -0.57 Wm^{-2}yr^{-1} for CERES) (Table S1). The seasonal difference in ARE trends agrees with that of AOD which shows a smaller decrease in winter (regression slope of -0.02 yr^{-1}) and a larger decrease in summer (-0.06 yr^{-1}). Also, this seasonal difference in ARE trends agrees with the seasonal difference in the trends of PM$_{2.5}$ discussed in our previous study (Leung et al., 2020), which found a much slower decrease in wintertime PM$_{2.5}$ (-3.2% yr^{-1}) since 2014, in contrast to a drastic summertime decrease (-10.3% yr^{-1}). This seasonal discrepancy is mainly because the wintertime aerosol decrease is buffered by unfavorable chemical processes associated with increased oxidants and insufficient NH$_3$ supply. In winter, the combined effect of the CRE increase and the relatively weak ARE decrease results in the decrease in SSR. On the contrary, the stronger ARE decrease and the concurrent CRE decrease in summer together lead to the rapidly increasing summertime SSR.

4. Conclusions and Implications

By using the ground-based and satellite-based observations, this study aims to examine the surface solar radiation (SSR) variations over eastern central China (ECC) after the implementation of the Clean Air Action plan in China in 2013, and, more importantly, to identify the relative contributions of aerosol radiative effect (ARE) and cloud radiative effect (CRE) to the SSR varying trends. The main conclusions are summarized as follows.

A significant increase tendency is revealed by the SSRs for both CERN and CERES datasets for 2014–2019 (Sen's slopes of 1.16 W m^{-2} yr^{-1} and 0.84 W m^{-2} yr^{-1} averaged at 17 stations, respectively). The SSR trend for 2014–2019 is larger than that for 2005–2019, which indicates that the recovery of SSR in China has accelerated after 2013. The SSR shows an increase over most of ECC, with the most significant increase occurring in northern and central parts of the domain (≥ 2 W m^{-2} yr^{-1}).

For both CERN and CERES datasets, the annual mean AREs present strongly declining trends. However, the annual mean CREs show insignificant trends with large fluctuations. These results indicate that the strongly declining ARE plays a dominant role in producing the upward annual SSR trends, and cloud variations should not be the main reason for the SSR increase over ECC.

Distinction exists in the trends of seasonal mean SSRs. Both the CERN and CERES observations show strong increasing trends with statistical significance in summer but decreasing trends in winter when the combination of strong CRE increase and weak ARE decrease results in decreasing SSR. In summer, the decrease trends in ARE could be attributed to the strongest declining of aerosol loading in this season.

In this paper, we conclude that after the implementation of stringent air pollution control actions in 2013, the recovery rates of SSR have been faster than ever before. Serious concerns over the negative health effects of severe air pollution, including from secondary aerosol precursors, continue to push China toward policies that aim to reduce aerosol concentrations (Schwarz et al., 2020). Given the success of current air pollution control policies, it is plausible that air pollutant emissions will continue to decline between now and 2030 (Cai et al., 2017), which will likely continue to recover SSR. The recent fastest-ever and ongoing SSR recovery over ECC is expected to significantly increase solar PV electricity generation potential. As a result, the air pollution control actions can lead to not only considerable environmental and health improvements, but also increases in solar photovoltaic energy production. This is potentially an important cobenefit of air pollution controls in China which deserves more attention in future decision making. Additionally, we do a preliminarily discussion on the trends in SSR over the northwest China, where large PV power plants are located. (shown in Text S3 and Figure s7).

Data Availability Statement

No new data are used in this work. The data from MODIS used in the present study can be obtained from https://ladsweb.modaps.eosdis.nasa.gov. The CERES data can be freely downloaded from https://ceres.larc.nasa.gov/. The CERN data that support the findings of this study are available through Liu et al. (2017). The PM$_{2.5}$ data are available through Wei et al. (2020, 2021).

References

Augustine, J. A., & Dutton, E. G. (2013). Variability of the surface radiation budget over the United States from 1996 through 2011 from high-quality measurements. *Journal of Geophysical Research: Atmospheres*, *118*, 43–53. https://doi.org/10.1029/2012JD018551

Bright, R. M., Cherubini, F., & Strømman, A. H. (2012). Climate impacts of bioenergy: Inclusion of carbon cycle and albedo dynamics in life cycle impact assessment. *Environmental Impact Assessment Review*, *37*, 2–11.

Cai, S., Wang, Y., Zhao, B., Wang, S., Chang, X., & Hao, J. (2017). The impact of the "Air Pollution Prevention and Control Action Plan" on PM2.5 concentrations in Jing-Jin-Ji region during 2012–2020. *The Science of the Total Environment*, *580*, 197–209. https://doi.org/10.1016/j.scitotenv.2016.11.188

Che, H. Z., Shi, G. Y., Zhang, X. Y., Arimoto, R., Zhao, J. Q., Xu, L., et al. (2005). Analysis of 40 years of solar radiation data from China, 1961-2000. *Geophysical Research Letters*, *32*, L06803. https://doi.org/10.1029/2004GL022322

CNREC (2014). *China wind, solar and bioenergy roadmap 2050-short version.* Available from http://www.cnrec.org.cn/english/publication/2014-12-25-457.html

Council, C. S. (2013). *Action plan on air pollution prevention and control (in Chinese).* Available from http://www.gov.cn/zwgk/2013-09/12/content_2486773.htm

Council, C. S. (2018). *Three-year action plan on defending the blue sky (in Chinese).* Available from http://www.gov.cn/zhengce/content/2018-07/03/content_5303158.htm

Ding, A., Huang, X., Nie, W., Chi, X., Xu, Z., Zheng, L., et al. (2019). Significant reduction of PM2.5 in eastern China due to regional-scale emission control: Evidence from SORPES in 2011–2018. *Atmospheric Chemistry and Physics*, *19*(18), 11791–11801. https://doi.org/10.5194/acp-19-11791-2019

Doelling, D. R., Loeb, N. G., Keyes, D. F., Nordeen, M. L., Morstad, D., Nguyen, C., et al. (2013). Geostationary enhanced temporal interpolation for CERES flux products. *Journal of Atmospheric and Oceanic Technology*, *30*(6), 1072–1090. https://doi.org/10.1175/jtech-d-12-00136.1

Doelling, D. R., Sun, M., Nguyen, L. T., Nordeen, M. L., Haney, C. O., Keyes, D. F., & Mlynczak, P. E. (2016). Advances in geostationary-derived longwave fluxes for the CERES synoptic (SYN1deg) product. *Journal of Atmospheric and Oceanic Technology*, *33*(3), 503–521. https://doi.org/10.1175/jtech-d-15-0147.1

Feng, F., & Wang, K. (2018). Merging satellite retrievals and reanalyzes to produce global long-term and consistent surface incident solar radiation datasets. *Remote Sensing*, *10*(1), 115. https://doi.org/10.3390/rs10010115

Folini, D., & Wild, M. (2015). The effect of aerosols and sea surface temperature on China's climate in the late twentieth century from ensembles of global climate simulations. *Journal of Geophysical Research: Atmospheres*, *120*, 2261–2279. https://doi.org/10.1002/2014JD022851

Forgan, B. W. (1996). A new method for calibrating reference and field pyranometers. *Journal of Atmospheric and Oceanic Technology*, *13*(3), 638–645. https://doi.org/10.1175/1520-0426(1996)013<0638:ANMFCR>2.0.CO;2

Gueymard, C. A. (2008). REST2: High-performance solar radiation model for cloudless-sky irradiance, illuminance, and photosynthetically active radiation - Validation with a benchmark dataset. *Solar Energy*, *82*(3), 272–285. https://doi.org/10.1016/j.solener.2007.04.008

Harris, I., Jones, P. D., Osborn, T. J., & Lister, D. H. (2014). Updated high-resolution grids of monthly climatic observations—The CRU TS3.10 Dataset. *International Journal of Climatology*, *34*(3), 623–642. https://doi.org/10.1002/joc.3711

Hu, B., Wang, Y., & Liu, G. (2007). Ultraviolet radiation spatio-temporal characteristics derived from the ground-based measurements taken in China. *Atmospheric Environment*, *41*(27), 5707–5718. https://doi.org/10.1016/j.atmosenv.2007.02.044

Leung, D. M., Shi, H., Zhao, B., Wang, J., Ding, E. M., Gu, Y., et al. (2020). Wintertime particulate matter decrease buffered by unfavorable chemical processes despite emissions reductions in China. *Geophysical Research Letters*, *47*, e2020GL087721. https://doi.org/10.1029/2020GL087721

Li, J., Jiang, Y., Xia, X., & Hu, Y. (2018). Increase of surface solar irradiance across East China related to changes in aerosol properties during the past decade. *Environmental Research Letters*, *13*(3), 034006. https://doi.org/10.1088/1748-9326/aaa35a

Li, Z., Lau, W. K.-M., Ramanathan, V., Wu, G., Ding, Y., Manoj, M. G., et al. (2016). Aerosol and monsoon climate interactions over Asia. *Reviews of Geophysics*, *54*, 866–929. https://doi.org/10.1002/2015RG000500

Li, Z., & Trishchenko, A. P. (2001). Quantifying uncertainties in determining SW cloud radiative forcing and cloud absorption due to variability in atmospheric conditions. *Journal of Atmospheric Science*, *58*(4), 376–389.

Li, X., Wagner, F., Peng, W., Yang, J., & Mauzerall, D. L. (2017). Reduction of solar photovoltaic resources due to air pollution in China. *Proceedings of the National Academy of Sciences of the United States of America*, *114*(45), 11867–11872. https://doi.org/10.1073/pnas.1711462114

Li, Z., Xia, X., Cribb, M., Mi, W., Holben, B., Wang, P., et al. (2007). Aerosol optical properties and their radiative effects in northern China. *Journal of Geophysical Research*, *112*, D22S01. https://doi.org/10.1029/2006JD007382

Liang, F., & Xia, X. A. (2005). Long-term trends in solar radiation and the associated climatic factors over China for 1961–2000. *Annales Geophysicae*, *23*(7), 2425–2432. https://doi.org/10.5194/angeo-23-2425-2005

Liu, H., Hu, B., Zhang, L., Zhao, X. J., Shang, K. Z., Wang, Y. S., & Wang, J. (2017). Ultraviolet radiation over China: Spatial distribution and trends. *Renewable and Sustainable Energy Reviews*, *76*, 1371–1383. https://doi.org/10.1016/j.rser.2017.03.102

Mann, H. B. (1945). Nonparametric tests against trend. *Econometrica*, *13*(3), 245–259. https://doi.org/10.2307/1907187

Perez, R., Ineichen, P., Seals, R., & Zelenka, A. (1990). Making full use of the clearness index for parameterizing hourly insolation conditions. *Solar Energy*, *45*(2), 111–114. https://doi.org/10.1016/0038-092x(90)90036-c

Qian, Y., Kaiser, D. P., Leung, L. R., & Xu, M. (2006). More frequent cloud-free sky and less surface solar radiation in China from 1955 to 2000. *Geophysical Research Letters*, *33*, L01812. https://doi.org/10.1029/2005GL024586

Ramanathan, V., Crutzen, P. J., Kiehl, J. T., & Rosenfeld, D. (2001). Atmosphere—Aerosols, climate, and the hydrological cycle. *Science*, *294*(5549), 2119–2124. https://doi.org/10.1126/science.1064034

Roderick, M. L., & Farquhar, G. D. (2002). The cause of decreased pan evaporation over the past 50 years. *Science*, *298*(5597), 1410–1411.

Rutan, D. A., Kato, S., Doelling, D. R., Rose, F. G., Le Trang, N., Caldwell, T. E., & Loeb, N. G. (2015). CERES synoptic product: methodology and validation of surface radiant flux. *Journal of Atmospheric and Oceanic Technology*, *32*(6), 1121–1143. https://doi.org/10.1175/jtech-d-14-00165.1

Sanchez-Lorenzo, A., Wild, M., Brunetti, M., Guijarro, J. A., Hakuba, M. Z., Calbo, J., et al. (2015). Reassessment and update of long-term trends in downward surface shortwave radiation over Europe (1939–2012). *Journal of Geophysical Research: Atmospheres*, *120*, 9555–9569. https://doi.org/10.1002/2015jd023321

Schwarz, M., Folini, D., Yang, S., Allan, R. P., & Wild, M. (2020). Changes in atmospheric shortwave absorption as important driver of dimming and brightening. *Nature Geoscience*, *13*(2), 110. https://doi.org/10.1038/s41561-019-0528-y

Shi, H., Li, W., Fan, X., Zhang, J., Hu, B., Husi, L., et al. (2018). First assessment of surface solar irradiance derived from Himawari-8 across China. *Solar Energy*, *174*, 164–170. https://doi.org/10.1016/j.solener.2018.09.015

Stanhill, G., & Cohen, S. (2001). Global dimming: A review of the evidence for a widespread and significant reduction in global radiation with discussion of its probable causes and possible agricultural consequences. *Agricultural and Forest Meteorology*, *107*(4), 255–278. https://doi.org/10.1016/s0168-1923(00)00241-0

Sun, H., Zhi, Q., Wang, Y., Yao, Q., & Su, J. (2014). China's solar photovoltaic industry development: The status quo, problems and approaches. *Applied Energy*, *118*, 221–230. https://doi.org/10.1016/j.apenergy.2013.12.032

Wang, Y., Duan, X., & Wang, L. (2019). Spatial-temporal evolution of PM2.5 concentration and its socioeconomic influence factors in chinese cities in 2014–2017. *International Journal of Environmental Research and Public Health*, *16*(6), 985. https://doi.org/10.3390/ijerph16060985

Wang, K., Ma, Q., Li, Z., & Wang, J. (2015). Decadal variability of surface incident solar radiation over China: Observations, satellite retrievals, and reanalyzes. *Journal of Geophysical Research: Atmospheres*, *120*, 6500–6514. https://doi.org/10.1002/2015JD023420

Wei, J., Li, Z., Cribb, M., Huang, W., Xue, W., Sun, L., et al. (2020). Improved 1 km resolution PM2.5 estimates across China using enhanced space-time extremely randomized trees. *Atmospheric Chemistry and Physics*, *20*(6), 3273–3289. https://doi.org/10.5194/acp-20-3273-2020

Wei, J., Li, Z., Guo, J., Sun, L., Huang, W., Xue, W., et al. (2019). Satellite-derived 1-km-resolution PM1 concentrations from 2014 to 2018 across China. *Environmental Science & Technology*, *53*(22), 13265–13274. https://doi.org/10.1021/acs.est.9b03258

Wei, J., Li, Z., Lyapustin, A., Sun, L., Peng, Y., Xue, W., et al. (2021). Reconstructing 1-km-resolution high-quality PM2.5 data records from 2000 to 2018 in China: Spatiotemporal variations and policy implications. *Remote Sensing of Environment*, *252*, 112136. https://doi.org/10.1016/j.rse.2020.112136

Wielicki, B. A. (1996). Clouds and the Earth's radiant energy system (CERES): An earth observing system experiment (vol 77, pg 860, 1996). *Bulletin of the American Meteorological Society*, *77*(7), 1590–1590.

Wild, M., Gilgen, H., Roesch, A., Ohmura, A., Long, C. N., Dutton, E. G., et al. (2005). From dimming to brightening: Decadal changes in solar radiation at Earth's surface. *Science*, *308*(5723), 847–850. https://doi.org/10.1126/science.1103215

Xia, X., Li, Z., Holben, B., Wang, P., Eck, T., Chen, H., et al. (2007). Aerosol optical properties and radiative effects in the Yangtze Delta region of China. *Journal of Geophysical Research: Atmospheres*, *112*, D22S12. https://doi.org/10.1029/2007JD008859

Zhai, S., Jacob, D. J., Wang, X., Shen, L., Li, K., Zhang, Y., et al. (2019). Fine particulate matter (PM2.5) trends in China, 2013–2018: Separating contributions from anthropogenic emissions and meteorology. *Atmospheric Chemistry and Physics*, *19*(16), 11031–11041. https://doi.org/10.5194/acp-19-11031-2019

Zhang, Q., Zheng, Y., Tong, D., Shao, M., Wang, S., Zhang, Y., et al. (2019). Drivers of improved PM2.5 air quality in China from 2013 to 2017. *Proceedings of the National Academy of Sciences of the United States of America*, *116*(49), 24463–24469. https://doi.org/10.1073/pnas.1907956116